Demonstration of a Palm-Sized 30 Watt Air-to-Power Turbine Generator

Citation: Sato, S., et al., "Demonstration of a Palm-Sized 30 Watt Air-to-Power Turbine Generator." Proceedings of ASME Turbo Expo 2010, June 14-18, 2010, Glasgow, UK, ASME, 2010: no. GT2010-22925 p. 459-70 doi 10.1115/GT2010-22925 ©2010 Author(s)

Published Version: 10.1115/GT2010-22925

Publisher: ASME International

Permanent Link: https://hdl.handle.net/1721.1/125892

Version: Final published version: final published article, as it appeared in a journal, conference proceedings, or other formally published context

Proceedings of ASME Turbo Expo 2010: Power for Land, Sea and Air
GT2010
June 14-18, 2010, Glasgow, UK

GT2010-22925

DEMONSTRATION OF A PALM-SIZED 30 WATT AIR-TO-POWER TURBINE GENERATOR

S. Sato, S. Jovanovic, J. Lang, Z. Spakovszky
Gas Turbine Laboratory
Massachusetts Institute of Technology
Cambridge, MA 02139

ABSTRACT

A compact, high power-density turbo-generator system was conceived, designed and experimentally tested. The air-to-power (A2P) device with a nominal design point of 50 W electric power output operates on high pressure air such as for example from a plant pneumatic system or a portable bottle of pressurized air. A concept design study was first carried out to explore the design space for a range of output power at cost efficiency levels specified in collaboration with industry. The cost efficiency is defined as the cost of electrical power over the cost of pressurized air. The key challenge in the design is the relatively low power demand of 50 W while operating at high supply pressures of nominally 5 to 6 bar. To meet the cost efficiency goal under these conditions, a high-speed turbine and generator (~450,000 rpm) are required with small blade span (~200 μm) minimizing the mass flow while achieving the highest possible turbine performance. Since turbines with such small turbomachinery blading aren't commercially available, a silicon-based MEMS turbine was designed using 2-D and 3-D CFD computations. To reduce the development time, existing and previously demonstrated custom-made generator and ceramic ball-bearing technology were used, resulting in a compact A2P proof-of-concept demonstration. The cylindrical device of 35 mm diameter resembles a tube fitting with a standard M24 adapter. Without load, a top turbine speed of 475,000rpm was demonstrated exceeding the design specification. Using load resistors, the proof-of-concept A2P device achieved 30 W of electrical power at 360,000 rpm and a turbine efficiency of 47%, meeting the cost efficiency goal. Higher speeds under load could not be achieved due to thrust load limitations of the off-shelf ball bearings. The demonstrated performance is in good agreement with the projected CFD based predictions. To the authors' knowledge, this is the first successful demonstration of a self-contained, 50 W-class turbo-generator of hybrid architecture where a MEMS turbine disk is joined with a precision machined titanium shaft and aluminum housing.

INTRODUCTION

With the ever growing need for portable and distributed power sources, small-scale devices ranging from a few Watts to several hundred Watts are currently being studied by various research groups. Most applications call for single-stage radial turbomachinery components and high-speed generators in the 50 to 500 Watt power range and yield challenges in fluid machinery design at low Reynolds numbers, micro fabrication, and rotordynamics and bearings for high-speed operation [1-2]. These challenges are of multi-disciplinary nature but one of the major hurdles is the reliable and efficient operation of small-scale fluid and electrical machinery. This is the focus of the present paper.

A number of related studies can be found in the literature. For example an air driven single-stage radial turbine of 12 mm diameter and 250 μm blade span, fabricated using mold shape deposition manufacturing (SDM), was successfully operated at 420,000 rpm [3]. The turbine rotor was supported by hybrid ball bearings and produced 72 W of shaft power. A 100 W class miniature gas turbine was developed at IHI and Tohoku University [4] where 5-axis micro-milling technology was employed to fabricate the 3-dimensional turbine blades required to achieve the target efficiency. In a turbocharger type arrangement the rotor shaft was levitated by hydro-inertia type gas bearings and operated at 770,000 rpm. Using an off-shelf dental drill, a samarium-cobalt (SmCo) based axial-flux permanent-magnet synchronous MEMS generator was operated at 305,000 rpm generating a net electric power output of 8 W [5]. The compact stator windings were electroplated and the brittle rotor magnet material was contained using a tight-fit containment hoop. An electro-discharge machined (EDM) 10 mm diameter, low pressure ratio axial turbine coupled to an off-the-shelf generator was tested at 160,000 rpm, generating 16 W electrical power-output [6]. A turbo-generator consisting of a 10 mm diameter micro-machined radial turbine with 590 μm blade span coupled to a high-speed generator was operated at 490,000 rpm delivering 150 W of net electric power output [7].

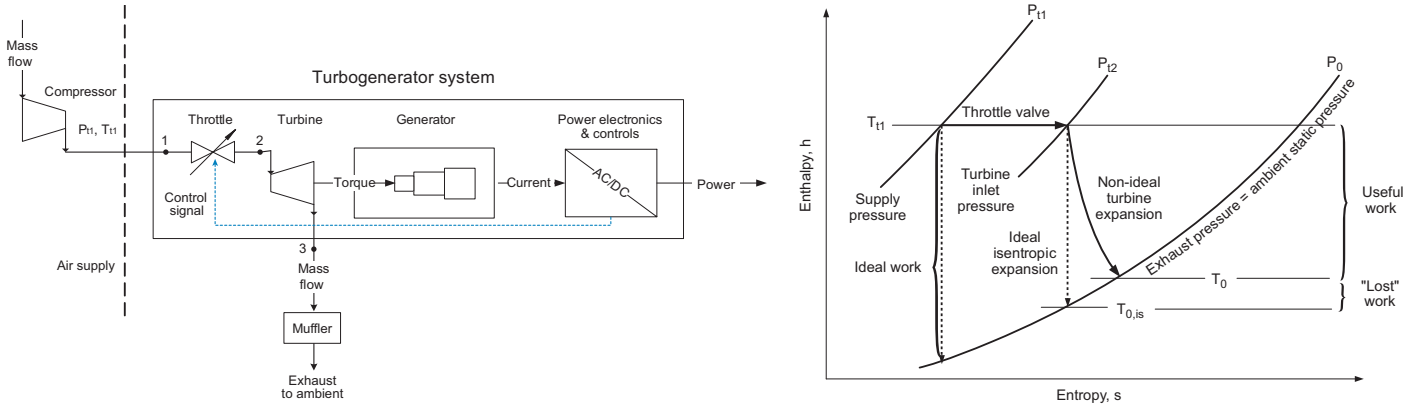

Fig. 1: Conceptual layout of air-to-power (A2P) system (left) and thermodynamic model (right).

The generator design employed an integral rotor design using a titanium sleeve containing the magnetic core material to ensure rotor integrity at high speed. Using a similar rotor architecture but an axial impulse turbine, the same research group reports on a turbo-generator system that demonstrates a power output of 124 W at a mass flow of 4.7 g/s and an inlet pressure of 6 bar [8]. The main challenges are a low turbine efficiency of 22% and the relatively high operating mass flow.

SCOPE OF PAPER

The present paper focuses on a miniature turbo-generator distributed power system that converts compressed air to electric power. The idea behind Air-to-Power (A2P) is that highly compact, high power density air turbo-generators permit local powering of automation electronics from plant pneumatic systems or consumer electronics and other equipment from portable pressurized air sources. The typical power demand for the above applications is in the range of 20 W to 60 W. The conceptual layout of a A2P turbo-generator system is depicted in Figure 1 and consists of a shut-off and throttle valve which modulates the air flow to the turbine, a turbine which drives a generator, power electronics[1] which transform the output of the generator to a form compatible with the customer load, a control system which modulates the air according to the customer demand and ensures safety, and a muffler to quiet the air exhaust. A major metric is the operating cost of the A2P approach relative to simply purchasing the electric power. The key objective of the work is to conceive, design and demonstrate a proof-of-concept device with a nominal power output of 50 W while meeting the cost efficiency[2] goal specified in collaboration with industry.

There are three major constraints which shape the design of such a device: manufacturing of the turbine, centrifugal stress in the generator, and bearings and rotor dynamics. The trade is between the turbine's need to turn fast and the generator's stress limitation (and therefore cost and complexity). Another important factor is the desire to have a single design that can operate well over a range of input pressures and power demands.

For this particular application and its design specification, the turbo-generator concepts reported in the literature are either overpowered, too low in efficiency, or consume too high a mass flow. As will be shown in the paper, efficiency scales with size, with higher system efficiencies possible at the larger sizes. For the overall system to be efficient the turbine must be designed to operate over a high pressure ratio (5:1 to 6:1) and low mass flow. In general, the efficiency of a single-stage turbine will drop with increasing pressure ratio, so there is a trade between turbine and system efficiency. Furthermore, the desire for low mass flows needed at these power levels yields turbine designs with relatively short blade spans, introducing manufacturing constraints and aerodynamic challenges.

A silicon-based MEMS turbine with planar geometry is considered and provides an effective match to the generator and obviates the manufacturing constraints. The concept is different from previous work in that the rotating machinery is of hybrid architecture where a planar silicon turbine disk is joined with a precision machined titanium shaft and aluminum housing. Furthermore, the concept achieves a relatively low mass flow at high efficiency compared to other devices in this power-class. The paper presents the details of the aero-thermodynamic and mechanical design of the A2P device and outlines its assembly and experimental testing. The experimental results are discussed with focus on turbine and generator performance, turbine rotor tip-clearance sensitivity, rotordynamic behavior of the shaft assembly, and overall performance of the proof-of-concept device.

A2P THERMODYNAMICS

As in any product, the operating cost is an important consideration, especially in relation to alternatives. In the case of the A2P concept, a useful comparison is between the cost of the air used compared to the cost for the same user power simply purchased, i.e. the overall cost efficiency. The thermodynamic concept of availability and the standard definitions of component (e.g. turbine and compressor) efficiencies were used as metrics to assess the system performance. A thermodynamic model in terms of an *h-s*

[1] Power electronics were not part of the demonstration presented here.

[2] The cost efficiency is defined as the cost of electrical power over the cost of pressurized air.

diagram is given in Figure 1 on the right. The ordinate indicates enthalpy, *h*, the available internal energy plus flow work of the fluid to be converted into useful work. The abscissa indicates entropy, *s*, which, for an adiabatic system, is related to the work dissipated or "lost" due to irreversibility.

Only the expansion through the turbine produces useful work. The pressure drop through the throttle valve or muffler gives rise to "lost" work, power unavailable to the customer. By their very nature, throttles generate a pressure drop by dissipation. Turbines are generally designed to work efficiently over only a relatively limited range of supply pressures. These considerations are especially important if a single design must operate efficiently at a variety of inlet pressures, either because different customers use different plant pressures or because the pressure at the A2P unit fluctuates significantly (perhaps due to other demands on the air supply). This analysis implies that, to the degree that operating cost is important to the success of the concept, care must be taken in designing components to maximize efficiency, and the turbine must be designed to utilize all of the pressure available in the plant air system. These two can be in some conflict in that the turbine designs, which maximize efficiency at one pressure ratio, are not usually the same that deliver good performance over a wide range.

DESIGN SPACE EXPLORATION

A concept design study was first carried out to explore the design space for 50 to 500 W output power at cost efficiency levels specified in collaboration with industry. To extract the maximum power from the high pressure air, a single-stage turbine must turn at the highest possible peripheral speed set by the strength limit of the turbine material. This speed is higher than the generator can withstand and implies that the turbine must be larger in diameter than the generator. But as the turbine diameter grows, the airfoil span must shrink to keep the flow area constant (for a given airflow rate). Calculations showed that the limitation of minimum airfoil height is reached below a turbine size of about 300 W. At smaller sizes then, constant airfoil span can result in a turbine with more area and thus more airflow than otherwise needed, leading to a loss of system efficiency. One conclusion from the design study is that *it is easier to design efficient turbines for the larger end of the design space under consideration, 500 W, than at the small end, 50 W.* One of the smallest conventionally manufactured turbocharger turbine wheels in the literature has a diameter of 10 mm, a blade span of 1.1 mm, and produces 340 W of shaft power at 870,000 rpm [9]. This rotational speed is too high for rolling contact bearings such that air bearings had to be used. It is important to note that, in the light of the cost efficiency goal, this blade span is too high and yields excessive mass flows as will be shown below.

In order to meet the cost efficiency design goal, the turbine mass flow must be reduced while increasing the specific shaft work capability to take advantage of the high supply pressure. The enabling design strategy is to trade blade span with rotor speed. For a choice of blade span, governed by manufacturing technology, the turbine flow area (and thus mass flow) can be reduced by reducing the turbine radius. Thus, for a given turbine architecture and specific turbine work, a higher shaft speed is required to meet the shaft power requirements. However, generator rotor balancing, mechanical stress and bearing considerations limit the maximum generator speed. Therefore, the integrated turbine and generator design must balance the blade manufacturability and generator speed constraints: the higher the rotor shaft speed, the less challenging the turbine design and the more challenging the generator design, and vice-versa.

Figure 2 analyzes in more detail the 50 W design space and the impact of different turbine manufacturing technologies, as well as the impact of different generator types, showing rotor diameter versus rotational speed. The left-hand graph describes the constraints for various generator types and the stress limitations of contained and uncontained rotor architectures. The hybrid ball bearing speed limit at 800,000 rpm is also marked for reference. The right-hand graph depicts the turbine design space and the range of available supply pressures (the solid and dashed black lines). The turbine assumptions are consistent with high-fidelity simulations outlined later and discussed in detail in [10]. The turbine blade span contours are marked in color and correspond to the minimum feature size achievable by the different manufacturing technologies

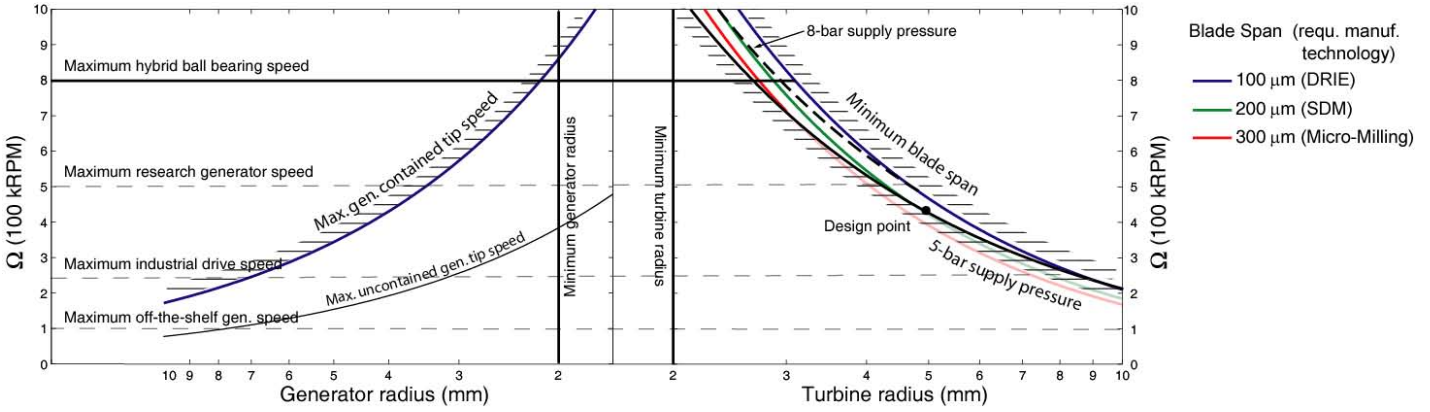

Fig. 2: 50 W turbo-generator design space with generator types and turbine blade manufacturing constraints.

considered: the 300 μm blade span corresponds to micro-milling, 200 μm correspond to SDM, and 100 μm correspond to Deep Reactive Ion Etching (DRIE). Note that DRIE can achieve smaller blade spans, but that efficiency considerations limit the minimum blade span to 100 μm. The major observation is that in this narrowly constrained design space only a DRIE manufactured MEMS turbine at high speeds yields a viable low-flow turbo-generator design. The black dot in the above figure indicates that the 50W power requirement can be met at a supply pressure of 5 bar using a silicon turbine design with 200 μm blade span and 10 mm diameter operating at 450,000 rpm. This requires a custom made generator as discussed next.

GENERATOR DESIGN SPACE

The generator design space is limited by several barriers. One barrier is an upper speed limit for the integrated turbine/generator rotor set by the choice of bearing technology. A second barrier is the minimum radius required to support the energy conversion of the turbine, and turbine construction. This limit is taken here to be near 2 mm. Further constraints are set by generator rotor manufacturing and mounting considerations where higher surface speeds can be achieved with containment hoops. Several high-performance, commercially-available generators were considered that can operate at high speeds, and at or above 50 W. These include 3 kW generators made by Calnetix, 100 W generators made by Aveox and a 50 W generator made by Maxon. Each of these generators sets a different high-speed limit. As a consequence of these limits, high-power operation necessarily results in larger diameter turbines operating at lower speeds deteriorating cost efficiency as discussed above. The detailed analysis showed that no commercially-available generator can meet the design requirements such that a custom-designed and fabricated generator was necessary.

Fortunately, such an experimental generator with integral rotor architecture was found to be available [7]. The rotor design uses a titanium sleeve to contain the magnetic core material, ensuring rotor integrity at high speed. The A2P system was designed and built around this 2-pole 3-phase wye-connected permanent-magnet synchronous machine capable of operating at speeds of at least 500,000 rpm, and torques of at least 1 mN-m. One challenge that remained with this generator was that its ball bearings were found to be incapable of standing off the axial loads of the reaction turbine, necessitating a compromised design of the A2P system[3].

[3] Given the short time frame of the project, the decision was made to use the ball bearings integral to the generator package in the concept demonstration. Future work includes the design of air journal- and thrust-bearings that are superior in performance and most suitable here since a pressurized air source is readily available. Note, that an impulse turbine would not lead to axial rotor loads but has inferior performance compared to a reaction turbine.

HIGH-WORK LOW-FLOW TURBINE DESIGN

From the scoping study above it is clear that the A2P turbine design requirements cannot be met by commercially-available turbines. A 2-D radial MEMS turbine is compatible with the blade span and rotor speed requirements and was considered for the proof-of-concept A2P device. This calls for a new, hybrid architecture where the silicon turbine disk is joined with a titanium shaft and aluminum housing. A high-work, low-flow turbine design operating near 450,000 rpm with a blade span, *L*, of 200 μm was designed with the goal to meet the required cost efficiency at 50 W electrical power output. An optimized, low reaction aerodynamic design enabled a high work coefficient at reasonable profile, endwall and tip-leakage losses in the low-aspect ratio blade passages as discussed next.

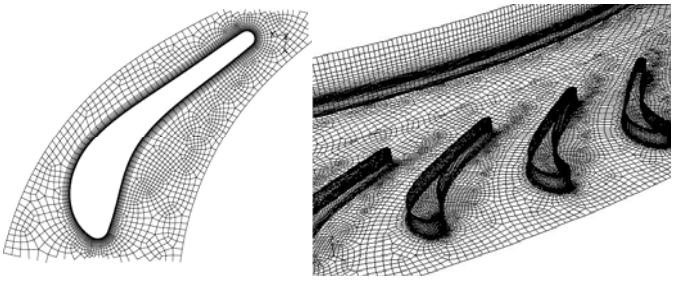

Fig. 3: 3-D CFD rotor O-mesh (not all cells are shown).

After the thermodynamic study discussed earlier, a mean-line analysis was carried out to define the velocity triangles and relevant pitch-wise averaged quantities. The stagnation pressure loss is modeled through loss coefficients corrected for Reynolds number effects at the small scale. Next, the turbine blade profiles were designed using MISES, a 2D coupled, viscous/inviscid Euler solver capturing profile losses and shock losses [11]. Since end-wall losses are dominant due to the relatively low blade aspect ratios of 0.2, 3D Reynolds Averaged Navier-Stokes (RANS) calculations of the entire turbine stage were carried out. The commercial code FLUENT was used for isolated stator and rotor flow simulations, where particular attention was paid to end-wall and secondary flow losses. The O-mesh type grid of the turbine rotor blades and the resulting turbine stage design are depicted in Figures 3 and 4. More details can be found in [10].

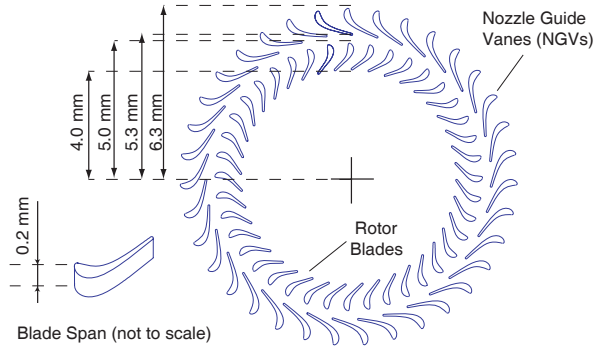

Fig. 4: High-pressure ratio, low-flow turbine design.

Table 1 summarizes the geometric and aero-thermodynamic design parameters.

Stator Vanes		Work coefficient	1.5
Aspect ratio (span/chord)	0.2	Flow coefficient	0.3
Solidity (chord/pitch)	2.0	Stage reaction	0.2
		Pressure ratio	5.0
Rotor Blades		Rotor rotational speed	450,000 rpm
Aspect ratio (span/chord)	0.2	Turbine shaft power	77 W
Solidity (chord/pitch)	2.4	Mass flow	1.45 g/s
Tip clearance (C/L)	0.1	Turbine efficiency	48 %

Table 1: A2P turbine design parameters

The rotor blade tip clearance C = 20 μm, which is the axial distance between the top of the rotor blade and the stationary casing (see Figure 7), results in stringent tolerance requirements of the micro-machined aluminum casing parts and challenges in device assembly as discussed later.

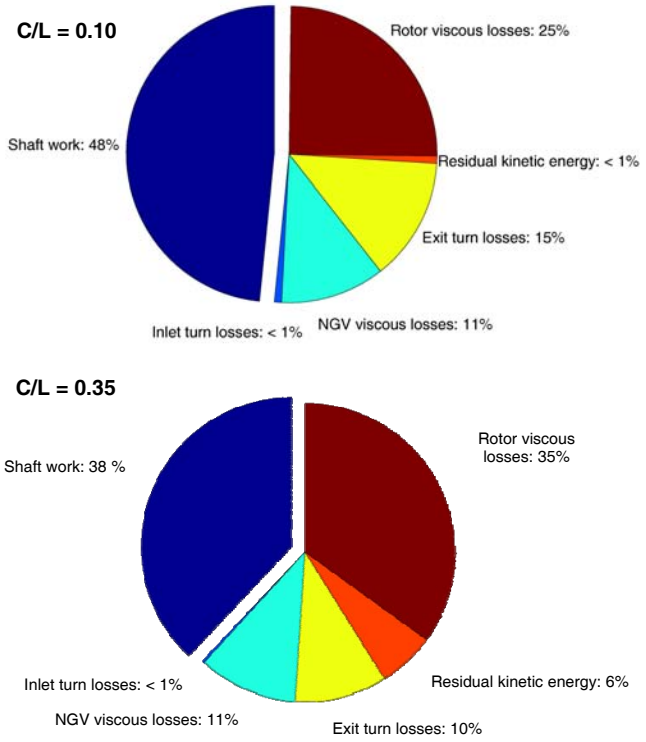

Fig. 5: 3-D CFD based turbine losses for design (top) and enlarged (bottom) blade tip-clearances.

3-D RANS calculations were also carried out to assess the turbine performance in the light of rotor blade tip-leakage losses. Computations were conducted at a nominal blade tip clearance of 20 μm (C/L = 0.1) and an enlarged blade tip clearance of 70 μm (C/L = 0.35), estimated from a preliminary machining tolerance analysis. The enlarged tip clearance yields enhanced tip leakage flow and increases the loss in the endwall region. The turbine performance was quantified in terms of entropy generated or the "lost" work.

Figure 5 summarizes the performance results for the two tip-clearance cases where the shaft work and the lost work are normalized by the ideal work. The computation at nominal tip-clearance results in turbine work output of 48% of the ideal work (adiabatic efficiency) due to viscous losses in the rotor blade row, in the stator or nozzle guide vanes (NGVs), in the exit turn, and residual kinetic energy. About 25% of the loss occurs in the rotor and is comprised of profile-, tip-leakage- and endwall losses. The NGV viscous loss is 11% and is governed by profile and endwall losses. The former scales with the cube of local free-stream Mach number and is relatively large due to the high-subsonic flow and relatively low average Reynolds number of 60,000. The tip-clearance loss is dramatically increased in the case of enlarged tip-clearances, increasing the rotor viscous losses by 10%. This results in 16 W of additional lost work reducing the turbine shaft power to 61 W and the adiabatic efficiency to 38%. Comparison to measured data is discussed in a later section.

MECHANICAL DESIGN & DEVICE ASSEMBLY

The device layout and the components of the A2P turbine-generator assembly are shown in Figure 6 together with a picture of the assembled device with the outlet cap removed. The A2P device is comprised of three main parts: the silicon turbine assembly, the generator components, and the outer casing. Turbine DRIE fabrication, device assembly and experimental testing were conducted at MIT's Gas Turbine Laboratory. The existing experimental generator with ball bearings was kindly provided by ETH [7] and all aluminum casing components were fabricated to high precision by Owens Inc. The silicon turbine rotor is mechanically connected to the titanium generator shaft via an alloy steel rotor adapter. The turbo-generator core components consist of the generator, the silicon stator, the stator holder which aligns the stator, and a shield which prevents the high-pressure air from leaking through the generator. Finally, these components are enclosed by an inlet cap, casing, and outlet cap with M2 bolts. O-rings are placed between the caps and the stator to seal the package. Shims can be inserted at two different locations in order to adjust the axial clearance between critical components.

The rotor and stator blade rows were fabricated from a two-wafer bonded stack. The top wafer was ultimately etched to form the turbine stator and rotor blades. The bottom wafer served as a structural support wafer. The radial clearance between the rotor disk and stator ring shown in Figure 7, is a critical dimension. It must be large enough to accommodate lateral excursions of the rotor, but it must not be too wide to avoid excessive leakage flows. Consequently, radial clearances ranging from 50 μm to 200 μm in 25 μm steps were etched in different rotor/stator pairs. The 150 μm radial clearance rotor-stator pair was selected as the best after the radial displacement of the rotor was measured during low and high-speed operation.

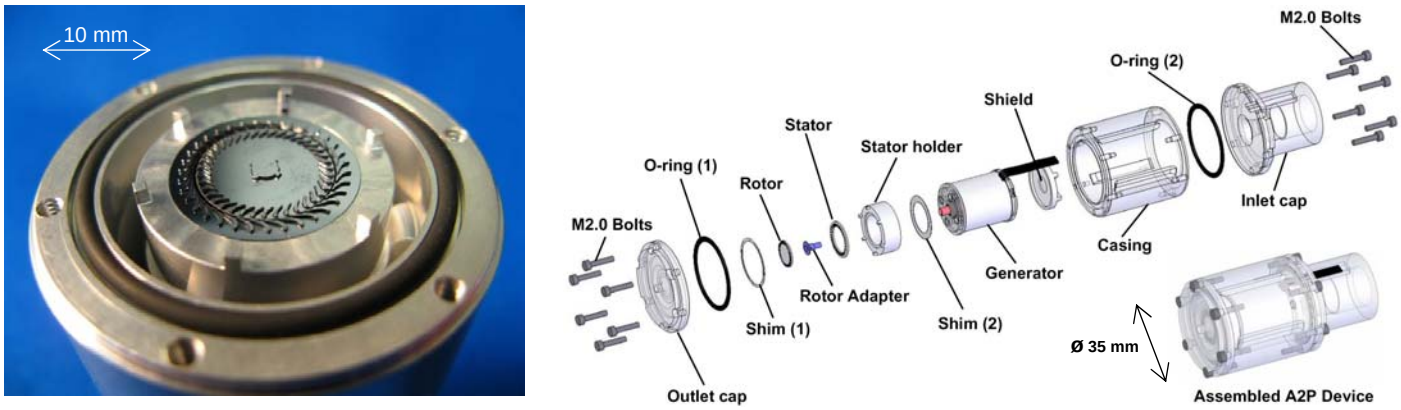

Figure 6: Silicon turbine (left) and exploded / assembled view (right) of 35 mm diameter 50W A2P turbo-generator.

Axial and Radial Component Alignment. A critical step in the A2P device assembly is the alignment of the different components. Misalignment of the rotor and stator not only impacts the aerodynamic performance of the turbine, but can also lead to destruction of the rotating parts.

Radial tolerances of the different A2P turbo-generator components were evaluated to identify the maximum and minimum possible misalignment of the turbine rotor. The alignment includes the ball bearing compliance, shaft-, adapter- and rotor-tolerances, and the radial tolerances of the motor casing, stator holder and stator ring. Combining the tolerance fits of the different parts, it was estimated that the radial clearance between the rotor disk and the stator ring might be reduced by as much as 46 µm from the nominal clearance. This information was combined with the measured radial deflection of the rotor shaft during operating to determine the required radial clearance between the stator and the rotor.

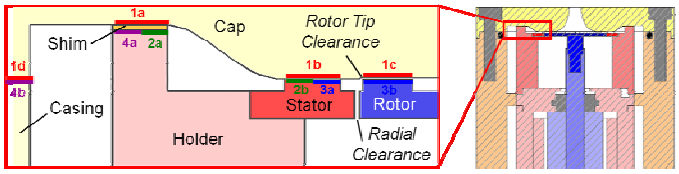

Fig. 7: Axial alignment of rotor and stator assembly.

There are three important dimensions that need to be carefully controlled for a successful device assembly and axial alignment. Referring to Figure 7 above: (i) the distance between the stator, stator holder and the outlet cap [1a, 1b and 2a, 2b] to ensure that the silicon stator is clamped between the stator holder and the outlet cap without being compressed and fractured; (ii) the distance between the rotor and the outlet cap [1b, 1c and 3a, 3b] to prevent the rotor from rubbing against the outlet cap during operation; and (iii) the distance between stator holder post and the casing [1a, 1d and 4a, 4b] to ensure the outlet cap is directly in contact with the stator holder post, without touching the casing.

In order to control the critical dimensions discussed above, shims were inserted at the following three locations: (i) between the stator holder post and the outlet cap (shim 1 in Figure 6) to control the distances 1a, 1b and 2a, 2b; (ii) between the stator holder and the generator casing (shim 2 in Figure 6) to control the distances 1b, 1c and 3a, 3b; and (iii) although not shown in Figure 6, an additional shim can be inserted between the inlet cap and the shield to adjust distances 1a, 1d and 4a, 4b if necessary.

To determine the adequate shim thickness required for alignment, each of the dimensions described above was measured at six different circumferential locations using an optical microscope, which has the capability to measure dimensions within +/- 2 µm. The measurements revealed significant circumferential variations between the different parts which were problematic for the outlet cap/stator holder/stator alignment, since a locally reduced clearance between the outlet cap and the stator holder can compress and fracture the silicon stator. To resolve this problem, the top of the silicon stator blades were treated with a room-temperature-vulcanizing (RTV) silicone coating of a few microns thickness. The compliant material ensures that clearance variations are compensated by the deformation of the protective coating.

ROTORDYNAMIC AND STRUCTUAL INTEGRITY CONSIDERATIONS

The high-speed operation of the A2P rotor assembly yields significant rotordynamic and structural integrity challenges. The most critical part in both radial alignment and power transmission is the precision machined rotor adapter that connects the titanium generator shaft with the silicon turbine disk. The backside of the rotor disk has a circular recess which sits on the center post of the adapter to align the two pieces as depicted in Figure 8. The stress distribution of the silicon rotor at high-speed operation was assessed using a Finite Element analysis in ANSYS. At 450,000 rpm, a stress concentration with a maximum value of 320 MPa at the corner of the centering recess was observed, exceeding the fracture strength of silicon of approximately 210 MPa. In order to relax this stress concentration, a supporting flange was incorporated in the adapter design. Only the flange is glued to the silicon disk transmitting the load while relieving the recess from stress concentrations. In order to determine the highest strength

adhesive for this application, various super glues and epoxys were tested on practice rotors. It was found that heat cured epoxy yields the best structural properties and highest strength. Assuming a perfect bond between the silicon rotor and the aluminum flange in the FEM analysis, the adapter flange reduces the maximum principal stress applied to the rotor to 90 MPa. This ensures the structural integrity of the turbine rotor assembly over the entire rotor speed range and even beyond design speed. The gluing did not impact the rotor balance as the glue weight is small compared to the weight of the adapter and magnetic rotor shaft.

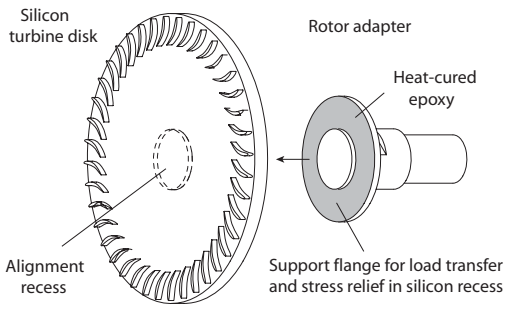

Fig. 8: Silicon turbine disk and rotor adapter.

High-Speed Structural Integrity Test. To demonstrate structural integrity of the rotor assembly, a silicon test rotor was spun successfully beyond its design speed of 450,000 rpm, operating the generator in motor mode. Figure 9 depicts the rotor speed measurement during the structural integrity experiment.

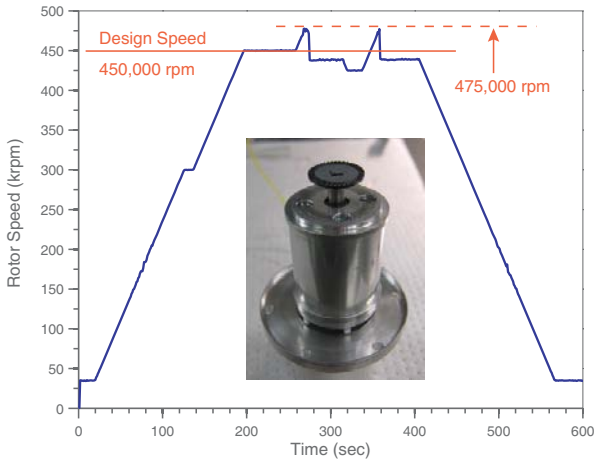

Fig. 9: Rotor structural integrity test at 475,000 rpm.

A sudden drop in motor speed was observed when attempting to accelerate to speeds higher than 475,000 rpm. This was attributed to the setup of the motor controller which is not used when running the turbine on air and generating power.

Rotordynamic Assessment. The investigation of the turbo-generator rotordynamics is necessary to determine the required shim thickness and operational rotor-stator radial clearance. Three dominant factors contribute to rotor shaft displacements: (1) bearing compliance, displacing the rotor towards the outlet cap due to turbine axial pressure loads[4], (2) rotor radial displacement due to shaft rigid-body and bending modes, and (3) rotor axial wobble through periodic variations of the turbine axial displacement due to possible tilt of the turbine surface relative to the shaft-adapter surface.

To quantify the axial shaft displacement due to turbomachinery thrust loads, a ball bearing compliance test was conducted using a high precision load cell. The measurements suggested shaft axial displacements of approximately 6 μm (34% of the blade tip clearance) at a nominal axial turbine load of 3 N and a pressure ratio of 5.

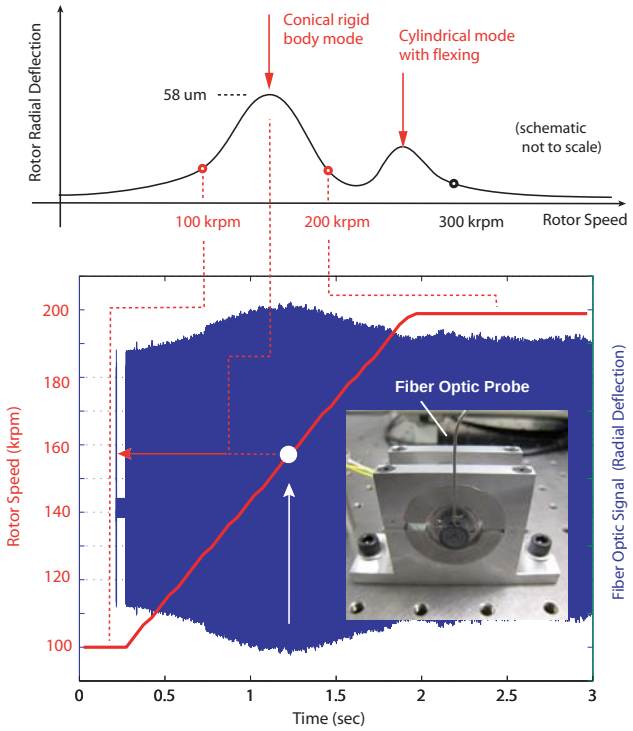

Fig. 10: Experimental measurement of rotor critical speeds during slow acceleration transients.

A Philtec fiber optic probe was used to measure the radial displacement of the rotor as shown in the inset of Figure 10. The probe was installed such that the surface of interest was in the near field of the probe, where the probe sensitivity is highest. To capture the transient behavior of the rotor, the shaft displacement was also recorded during acceleration transients from 0 to 50,000 rpm, 100,000 to 200,000 rpm (shown in Figure 10), and 200,000 to 300,000 rpm (not shown). At least two test runs at each of these conditions were conducted for

[4] As mentioned earlier, a thrust bearing could not be implemented without major changes to the generator assembly, introducing challenges in rotor axial alignment and stable operation.

repeatability. The maximum recorded radial displacement was 58 µm when accelerating the rotor from 100k to 200k rpm. This occurs when the turbine passes through one of the critical frequencies of the rotor system. Figure 10 also depicts a schematic of the radial displacement as a function of rotor speed (top) and the measured variation of radial displacement over time in blue for a rotor accelerating from 100,000 to 200,000 rpm (bottom). The measurements indicate the maximum displacement at approximately 160,000 rpm. This rotor frequency corresponds to the first rigid body mode frequency of the shaft. A direct-stiffness based rotordynamic analysis was conducted and the frequency of the conical rigid body mode is estimated at 169,000 +/- 15,000 rpm, in good agreement with the measurements. The computed modeshapes are depicted in Figure 11. Note that the second mode at 263,000 rpm is a cylindrical mode with some flexion due to the slender rotor architecture. The first full bending mode is estimated at 590,000 rpm well above the design speed. Combining this displacement measurement with the radial manufacturing tolerances, it was determined that a radial clearance of 100 µm was sufficient to avoid rotor-stator contact. Using a safety factor of 50%, silicon rotors with radial clearance of 150 µm were used in the experiments.

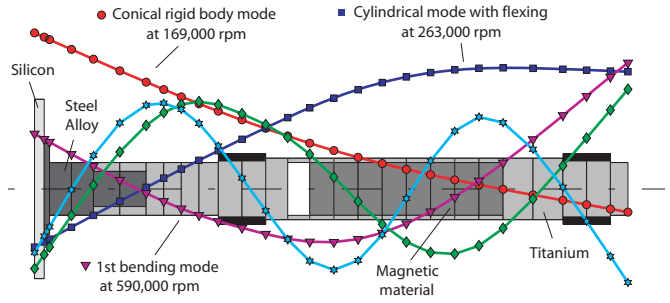

Fig. 11: Computed modeshapes at critical speeds.

Using a similar approach, the axial wobble of the turbine was also quantified. To avoid potential errors in the fiber optic measurement, the probe was placed at a slightly smaller radius than the turbine blades. Since the main contribution of the axial wobble is due to the turbine top surface not being perfectly perpendicular to the axis of rotation, the axial displacement is directly proportional to the distance from the center of the rotor. To estimate the actual displacement at the tip of the rotor, the axial displacement was scaled up based on the position of the probe and the rotor radius. The maximum axial wobble was observed during startup below 50,000 rpm, with a peak axial displacement of +/- 48 µm. The initial shim size was chosen based on this result, including a safety factor. The shim thickness was then adjusted during the experiment due to additional bearing compliance under rotation as only the static bearing compliance could be measured.

In summary, the alignment measurements and rotordynamic characterization lead to the following shim sizes for the assembled A2P device. Returning to Figure 6, shim (1) of 13 µm thickness was used to ensure sufficient clearance between the stator holder and the outlet cap to avoid the silicon stator to be compressed. For best performance, the thickness of shim (2) was 275 µm. This rather large shim size was based on experimental trial and error tests as the static bearing compliance tests dramatically underestimated the ball bearing stiffness during high-speed operation. The problem was conjectured to be due to ball bearing pre-load issues and, most importantly, the lack of a thrust bearing.

INSTRUMENTATION AND TEST SETUP

All experiments were conducted in the micro-engine test facility at MIT's Gas Turbine Laboratory. The working gas was nitrogen supplied from a gas bottle. The high-pressure gas was first throttled via a main valve and then passed through a pair of needle valves to allow for coarse and fine adjustments of the turbine inlet pressure. The inlet stagnation pressure and stagnation temperature were measured via a Kulite pressure transducer and a thermocouple as shown in the inset of Figure 12. In order to avoid contamination of the device from foreign particles[5], a 5 µm filter was placed in the supply pipe, upstream of the pressure transducer. The nitrogen mass flow was computed from Rotameter volume flow measurements.

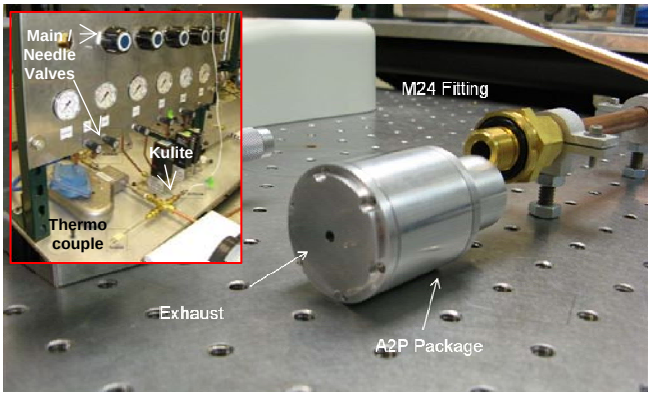

Fig. 12: A2P test setup and instrumentation.

The generator was operated without power electronics. Rather, it was set to drive a 3-phase wye-connected low-inductance resistive load. The power dissipated in the load resistors was considered to be the useful power delivered by the proof-of-concept A2P system. In an actual implementation, the resistive load would be replaced with a unity-power-factor AC-to-DC inverter. Such an inverter should be capable of operating at the 25-50 W power level with an efficiency in excess of 93% as for example reported in [12].

Phase voltage amplitude measurements across the load resistors were used to determine the device output power, and the electrical frequency produced by the generator allowed determining the mechanical speed of the turbine. To monitor the temperature of the generator and the bearings, the device

[5] Due to the small scale of the turbomachinery, particle contamination is a concern in real working environments and the use of an inlet filter is critical.

casing temperatures were also measured. The device inlet total pressure, inlet total temperature, exit static pressure and nitrogen volume flow were measured to compute the adiabatic efficiency of the turbine and the cost efficiency of the device.

EXPERIMENTAL RESULTS

Power generation tests were conducted with two different sets of load resistors and various shim thicknesses between the stator holder and the motor front flange to investigate generator electric efficiency and the sensitivity of turbine performance to blade tip-clearance effects and tip leakage flows.

Generator Performance. Two sets of experiments were conducted with the A2P system. During the first set of experiments, the load resistors were chosen to provide a 0.5 Ω line-to-neutral resistance so as to approximately match the 0.58 Ω line-to-neutral resistance of the generator. It was expected that this load would yield the maximum useful output power, although with an efficiency near only 50%. However, it was discovered that the internal inductance of the generator substantially limited the output power above 125,000 rpm, and so high-power operation with acceptable cost efficiency was not achieved. In response, a second set of experiments were run with load resistors providing a 2.2 Ω line-to-neutral resistance. This load increased the speed at which the generator inductance became important to approximately 300,000 rpm, thereby permitting an increase in output power, while also increasing the generator efficiency to 81%.

The power generated by the A2P turbo-generator was computed from the voltage measured between the load resistors and summed over the three phases. Figure 13 depicts the power delivered by the A2P system to the two different sets of resistive loads.

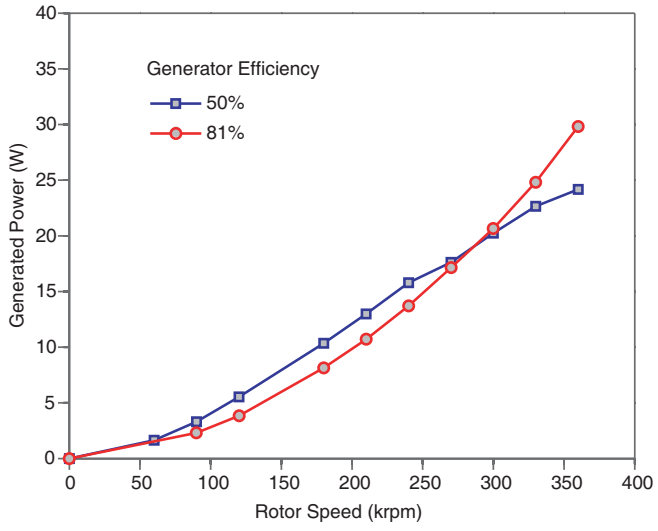

Fig. 13: Measured generator power vs. rotor speed for two different sets of load resistor banks.

The blue curve represents the delivered power for the experiments with a matched resistive load and an electrical efficiency of the A2P system of only 50%. As expected the delivered power grows quadratically with rotor frequency at low speeds. However, due to the generator phase inductance, the delivered power increases almost linearly above approximately 125,000 rpm. This reduced growth in power, combined with a 50% electrical efficiency, resulted in poor cost efficiency as will be shown later. In response, the load resistances were increased in order to both increase the electrical efficiency of the A2P system, and to raise the speed at which the phase inductance had a detrimental impact on delivered power output. The resulting power curve is marked red in Figure 13. At low speeds, the red curve falls beneath the blue curve since the matched load results in the greatest output power. However, at high speeds, the generator phase inductance begins to limit delivered power, and at speeds above approximately 275,000 rpm, the power delivered to the un-matched load (red) is increased. The higher generator efficiency of 81% also improves the cost efficiency of the A2P system. Note that the greatest power delivered to the load resistors was 30 W at 360,000 rpm.

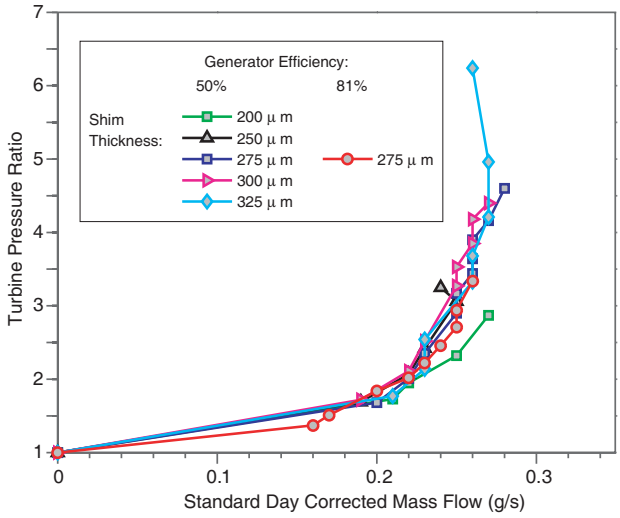

Fig. 14: Turbine pressure ratio vs. corrected mass flow for various rotor tip-clearances (adjusted with shims).

Turbine Performance. The measured turbine performance for different shim thicknesses and generator efficiencies is summarized in Figure 14. The performance is plotted in terms of standard day corrected mass flow, defined as $\dot{m}_{corr} = \dot{m}\sqrt{T_{t1}/T_{ref}}\,/\,(p_{t1}/p_{ref})$, and pressure ratio at various rotor speeds in order to collapse the different curves. Deviations are due to measurement errors and possible air leaks through the O-ring between the outlet cap and the casing[6]. Note that the standard day corrected mass flow becomes independent of

[6] The O-ring recess in the casing was designed for thinner shims than were used in the experiments due to bearing compliance issues. This led to reduced O-ring compression and flow leakage at high supply pressure settings.

pressure ratio at a value of about 2.5, indicating that the stator vanes are choked. The best performance with the least amount of leakage flow[7] was achieved with a shim thickness of 275 µm.

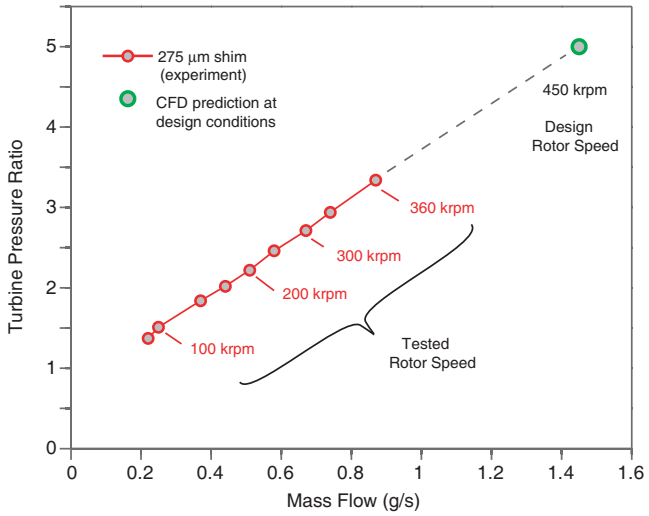

Fig. 15: Measured turbine pressure ratio vs. physical mass flow and predicted design point (CFD).

Figure 15 depicts the pressure ratio as a function of physical mass flow for this case. For reference, the different rotor speeds are also marked. At 360,000 rpm and a pressure ratio of 3.34, the consumed physical mass flow was 0.87 g/s. Higher speeds could not be achieved due to bearing compliance issues under load as discussed earlier. The predicted design condition is at 450,000 rpm and a pressure ratio of 5.0, yielding a mass flow of 1.45 g/s. Extrapolating the measured performance suggests reasonable agreement with the CFD predictions.

Determining the adiabatic efficiency of the turbine was challenging as there is heat transfer from the generator via conduction and convection and not all thermodynamic states or the direct turbine shaft power could be measured. Furthermore, the blockage in the stator passage can change between the test conditions when assembling and disassembling the device as the RTV protective coating might be squeezed differently.

The adiabatic turbine efficiency was estimated based on the measured generator shaft power and the isentropic stagnation enthalpy drop. The air flow over the inner casing cools the generator and it was assumed that all of the dissipated generator power is transferred to the turbine supply air. The stagnation enthalpy at turbine inlet was then calculated based on first law considerations and the estimated generator efficiency and measured power output. The isentropic enthalpy drop across the turbine was then calculated based on the inlet stagnation enthalpy and the estimated outlet static temperature assuming an adiabatic reversible expansion to atmospheric pressure. The turbine shaft power was computed from the measured generator output electrical power and generator efficiency. It has to be mentioned that the deduced adiabatic efficiency is underestimated since the isentropic stagnation enthalpy drop is overestimated by neglecting the residual kinetic energy at turbine exit and by assuming all the dissipated power in the generator is transferred to the supply air.

Based on the above, Figure 16 depicts the estimated adiabatic efficiency deduced from the measurements for a shim thickness of 275 um. A turbine adiabatic efficiency of 47% is estimated at 360,000 rpm and a pressure ratio of 3.34. The efficiency trend is in agreement with CFD predictions which are shown at design conditions for the two different blade tip clearances of 10% and 35% of blade span discussed earlier. Additional experiments are required to fully assess the running blade tip-clearance at design conditions.

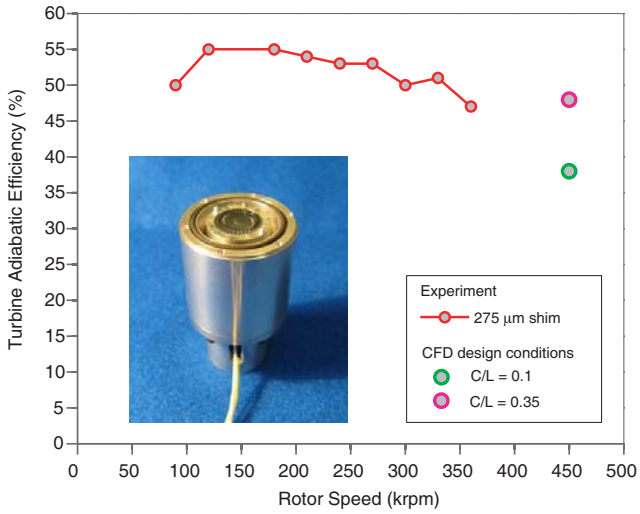

Fig. 16: Measured turbine adiabatic efficiency as a function of rotor speed and CFD predictions at design conditions for two blade tip clearances.

Overall A2P Device Performance. The main performance metric of interest is the cost efficiency of the air-to-power turbo-generator. The cost efficiency is defined as the cost per annum of electricity over the cost per annum to pressurize air to 6 bar, which is subsequently used to generate power. The latter depends on the mass flow consumed by the A2P device and its efficiency extracting shaft power from high pressure air and converting it into electrical power. The cost efficiency was determined based on the measurements as a function of rotor speed and the results in Figure 17 demonstrate that, with a generator efficiency of 81%, the cost efficiency goal is achieved and can even be exceeded. The actual values cannot be cited due to sponsor constraints.

[7] For shim thicknesses of 200 µm and 250 µm, the rotor blades touched the casing at pressure ratios higher than 3 and 3.25 respectively. Excessive leakage was observed for a shim thickness of 325 µm which is also indicated by an overall pressure ratio greater than 6.0 at the highest loading condition.

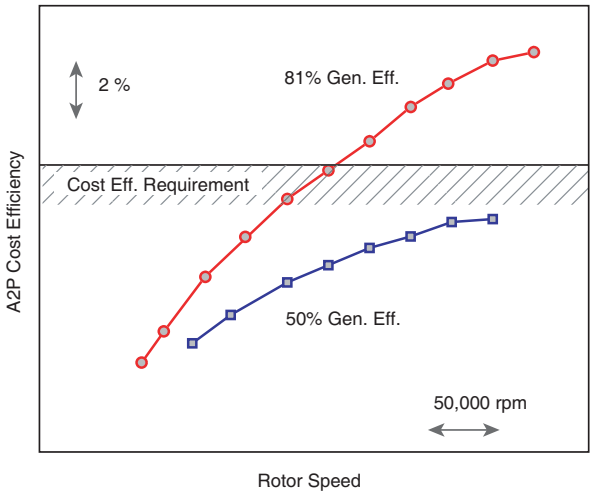

Fig. 17: A2P cost efficiency as a function of rotor speed for two different generator efficiencies.

SUMMARY AND CONCLUSIONS

A compact, high power-density A2P turbo-generator system was conceived, designed and experimentally tested. A concept design study was carried out first to explore the design space. The analysis showed that, in order to meet the cost efficiency goal at 50 W electrical power output, a high-work low-flow turbine with small blade span is required. Since turbines with blade spans of 200 µm aren't commercially available, a 2-D radial MEMS turbine compatible with the blade span and rotor speed requirements was considered for the demonstration of the proof-of-concept A2P device. An optimized, low reaction turbine enabled a high work coefficient and low flow coefficient design. Furthermore, the concept achieves a relatively high efficiency compared to other devices in this power-class. To reduce the development time, existing and previously demonstrated custom-made generator and bearing technology were used, resulting in a more compact A2P device with a new hybrid architecture where the silicon turbine disk is joined with a titanium shaft and aluminum housing.

The cylindrical device of 35 mm diameter, resembling a tube fitting with a standard M24 adapter, was experimentally tested using nitrogen from a high pressure tank. The proof-of-concept A2P device achieved 30 W of electrical power at 360,000 rpm and a turbine efficiency of 47%. This corresponds to a power density of 2.4 W/cm^3 not including the adapter flange of the inlet cap. Furthermore, the measured turbine performance at extrapolated design conditions is in reasonable agreement with the CFD predictions. The main challenges and limitations in the experimental demonstration are the commercially available high-speed ball bearings. The lack of an axial thrust bearing strongly impacted the operation of the device at high-loading conditions, requiring additional shims to avoid the rotor blades contacting the casing. To the authors' knowledge, this is the first successful demonstration of a self-contained, 50 W-class turbo-generator of this kind.

ACKNOWLEDGMENTS

The authors would like to kindly thank: Dr. Bernard Yen, James Letendre, David Otten, for their invaluable help in fabrication, assembly, and testing; Prof. Alan Epstein for the discussions in the early phase of the project, and Dr. Jürg Schiffmann for conducting the rotordynamic modeling; Andy Loomis at Lincoln Laboratories for help with the DRIE masks; Mark Plesniak at Owens Inc. for manufacturing the high-precision aluminum components; Daniel Krähenbühl, Dr. Christof Zwyssig, and Prof. Johann Kolar at ETH Zürich for kindly providing the generator assembly. Special thanks go to Jürgen Fuchs and Kai Garrels at ABB Stotz-Kontakt GmbH, and Dr. Christian Schroll and Dr. Peter Krippner at ABB Corporate Research Center Germany for initiating this project and for their constant support. This research was funded by ABB which is gratefully acknowledged.

REFERENCES

[1] Jacobson, S. "Aerothermal Challenges in the Design of a Microfabricated Gas Turbine Engine." AIAA Paper AIAA-98-2545, 1998.

[2] Kolar, J., Zwyssig, C., and Round, S., "Beyond 1,000,000 rpm - Review of Research on Mega-Speed Drive Systems." Proceedings of the 9th Brazilian Power Electronics Conference (COBEP'07), Blumenau, Brazil, Sept. 30 - Oct. 4, 2007.

[3] Tsuru, H., Sangkyun, K., Johnston, J., Toshiyuki, A., Matsunaga, M., and Prinz, F., "Challenges to Develop Miniature Gas Turbine Engine with Ceramic Unitary Compressor/Turbine Rotor". JSME International Symposium on Micro-Mechanical Engineering, Vol. 2003(20031130), pp. 296-305, 2003.

[4] Isomura, K., Tanaka, S., Togo, S., and Kanebako, H., "Development of Micromachine Gas Turbines at Tohoku University". In *Micro Gas Turbines*, Educational Notes RTO-EN-AVT-131, Paper 10, pp. 10-1 – 10-34, 2005.

[5] Arnold, D., Galle, P., Herrault, F., Das, S., Lang, J., and Allen, M., "A Self-Contained, Flow-Powered Microgenerator System." Tech. Dig. 5th Int. Workshop Micro Nanotechnology for Power Generation and Energy Conversion Apps. (PowerMEMS 2005), Tokyo, Japan, pp. 113-115, November 2005.

[6] Peris, J., Reynaerts, D., and Verplaetsen, F., "Development of an Axial Microturbine for a Portable Gas Turbine Generator." J. Micromech. Microeng. Vol. 13, S190-S195. 2003.

[7] Zwyssig, C., and Kolar, J.W., "Design Considerations and Experimental Results of a 100 W, 500,000 rpm Electrical Generator". J. Micromech. Microeng. Vol. 16, pp. 297-302, 2006.

[8] Krähenbuhl, D. Zwyssig, C. Hörler, H. Kolar, J.W. "Design Considerations and Experimental Results of a 60 W Compressed-Air-to-Electric-Power System". IEEE/ASME International Conference on Mechtronic and Embedded Systems and Apps. (MESA 2008), Beijing China, pp. 375-380, October 2008.

[9] Isomura, K., Murayama, M., Teramoto, S., Hikichi, K., Endo, Y., Togo, S., and Tanaka, S., "Experimental verification of the feasibility of a 100 W class micro-scale gas turbine at an impeller diameter of 10 mm," J. Micromech. Microeng., Vol. 16, pp. 254–261, 2006.

[10] Jovanovic, S., "Design of a 50 Watt Air Supplied Turbogenerator," MIT Master's Thesis, Department of Aeronautics and Astronautics, March, 2008.

[11] Drela, M., and Youngren, H. A User's Guide to MISES 2.59. 2006.

[12] Krähenbühl, D., Zwyssig, C., Bitterli, K., Imhof, M., and Kolar, J., "Evaluation of ultra-compact rectifiers for low power, high-speed, permanent-magnet generators," IECON Proceedings, pp. 453 – 460, 2009.